

Optical properties of self-organized wurtzite InN/GaN quantum dots: A combined atomistic tight-binding and full configuration interaction calculation

N. Baer,¹ S. Schulz,² S. Schumacher,² P. Gartner,^{1,3} G. Czycholl,² and F. Jahnke¹

¹*Institute for Theoretical Physics, Semiconductor Physics Group, University of Bremen, 28334 Bremen, Germany*

²*Institute for Theoretical Physics, Solid State Theory Group, University of Bremen, 28334 Bremen, Germany*

³*National Institute of Materials Physics, PO Box MG-7, Bucharest-Magurele, Romania*

(Dated: November 20, 2018)

In this work we investigate the electronic and optical properties of self-assembled InN/GaN quantum dots. The one-particle states of the low-dimensional heterostructures are provided by a tight-binding model that fully includes the wurtzite crystal structure on an atomistic level. Optical dipole and Coulomb matrix elements are calculated from these one-particle wave functions and serve as an input for full configuration interaction calculations. We present multi-exciton emission spectra and discuss in detail how Coulomb correlations and oscillator strengths are changed by the piezoelectric fields present in the structure. Vanishing exciton and biexciton ground state emission for small lens-shaped dots is predicted.

PACS numbers: 78.67.Hc, 73.22.Dj, 71.35.-y

In recent years, semiconductor quantum dots (QDs) have been the subject of intense experimental and theoretical research. As a new material system, group-III nitride based devices are of particular interest due to their wide range of emission frequencies from red to ultraviolet and their potential for high-power electronic applications^{1,2}. Being a technologically promising system, we study self-assembled InN/GaN QDs, which are typically grown by molecular beam epitaxy in Stranski-Krastanov growth mode. A theoretical description of the one-particle states in terms of a tight-binding (TB) model is presented, which provides a powerful approach to the electronic states of low-dimensional heterostructures on an atomistic level^{3,4}. For the calculation of optical absorption and emission spectra, full configuration-interaction (FCI) calculations^{5,6} are used to obtain a consistent description of correlated many-particle states. The calculation of dipole and Coulomb matrix elements from the TB one-particle wave functions facilitates the combination of these two approaches and allows us to investigate optical transitions between the interacting many-particle states of a QD with parameters obtained from a microscopic model. For the investigated small lens-shaped InN/GaN QDs, we report a negligible exciton and biexciton ground state emission whereas at higher excitation conditions strong emission from three to six exciton complexes is obtained.

We consider lens-shaped InN QDs, grown in (0001)-direction on top of an InN wetting layer (WL) and embedded in a GaN matrix. Their circular symmetry around the z -axis (diameter $d = 4.5$ nm, height $h = 1.6$ nm) preserves the intrinsic C_{3v} symmetry of the wurtzite crystal. For the WL we assume a thickness of one lattice constant. We apply a TB-model with an sp^3 basis $|\alpha, \mathbf{R}\rangle$, i.e., one s-state ($\alpha = s$) and three p-states ($\alpha = p_x, p_y, p_z$) per spin direction at each atom site \mathbf{R} . In contrast to most other III-V and II-VI semiconductors, one can neglect spin-orbit coupling and crystal-field splitting in InN and GaN^{2,7}. We include

non-diagonal elements of the TB-Hamiltonian matrix up to nearest neighbors and use the two-center approximation of Slater and Koster⁸ which yields 9 independent TB-parameters. These parameters are empirically determined such that the characteristic properties of the bulk bandstructure^{9,10} in the vicinity of the Γ point are reproduced. With these TB-parameters, the QD is modeled on an atomistic level where the parameters for each site are set according to the occupying atoms (N, In, Ga). At the InN/GaN interfaces averages of the parameters are used and effects of the surfaces in the finite-size supercell are removed¹¹. The spontaneous polarization in the wurtzite crystal structure lies within growth direction: $\mathbf{P} = P\mathbf{e}_z$. Additionally, a strain-induced piezoelectric field occurs that is quite strong for the investigated InN/GaN heterostructures. The piezoelectric field is determined by solution of the Poisson equation. The strain contribution to the polarization is approximated in a way following Ref. 12. For our chosen dot geometry, even a more sophisticated inclusion of strain effects¹³ will generate merely small lateral contributions to the piezoelectric field¹⁴, which are therefore neglected in the following. Lattice mismatch parameters and strain tensors are taken from Ref. 15, the small thermal strain contribution is neglected¹². The calculation yields a reasonable value of 5.5 MV/cm for the electric field inside the QD. The resulting electrostatic potential is included in the TB model as a site-diagonal potential $V_p(\mathbf{r}) = -e_0\phi_p(\mathbf{r})$. This method has successfully been applied to quantum well¹⁶ and QD¹⁴ structures before. By including the piezoelectric field the quantum confined Stark effect (QCSE) and its influence on the Coulomb matrix elements and the oscillator strengths can be studied.

The discussed QD confines three bound states for the electrons. They are included in the FCI calculations, together with the three lowest one-particle hole states that are spectrally well separated from the other localized hole states. These three one-particle states for the electrons and holes and their energies are depicted in Fig. 1. As

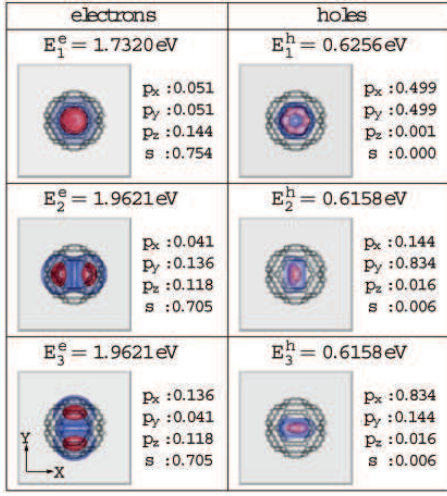


FIG. 1: (Color online). The QD geometry is shown from atop. The structure is visualized and isosurfaces of the charge density for the three energetically lowest electron (left) and hole (right) states are included for 10% (blue) and 50% (red) of the maximum value. For the holes the atomistic structure of the wurtzite crystal becomes most apparent for the excited p-states. The corresponding energies ($E_{1,2,3}^{e,h}$) of electron and hole states measured from the valence band maximum of bulk GaN and the atomic orbital character for each wave function are given. The dominant contributions are highlighted.

the lowest state for electrons and holes is invariant under rotation by $2\pi/3$, it is denoted as s-state. The two excited states are classified as p-states according to their symmetry properties and their two-fold degeneracy. The hole states show a strong band mixing visible in the orbital character (Fig. 1), which is in agreement with other multi-band approaches^{7,17}.

As emphasized above, a TB model represents an atomistic approach to describe the electronic structure of low-dimensional heterostructures. However, explicit knowledge about a basis set of localized Wannier states is not required for the calculation of one-particle energies and wave functions. Only the basic assumptions about the localized (atomic) orbitals, i.e. symmetry, spatial orientation⁸, and orthogonality, enter the TB Hamiltonian. Nevertheless, for the calculation of dipole and Coulomb matrix elements one needs – in principle – the localized basis states. For the Coulomb matrix elements, however, which are dominated by long-range contributions, the explicit knowledge of the atomic orbitals is in practice not required. This is because the structure of the localized orbitals is of significance only for on-site and nearest-neighbor interactions, which contribute less than 5% to the total Coulomb matrix elements. These findings are in agreement with Ref. 18. Thus, the matrix elements are approximated by a sum over the TB coefficients at atom sites \mathbf{R}, \mathbf{R}' with orbital indices α, β :

$$V_{ijkl} = \sum_{\mathbf{R}\mathbf{R}'} \sum_{\alpha\beta} c_{\mathbf{R}\alpha}^{i*} c_{\mathbf{R}'\beta}^{j*} c_{\mathbf{R}'\beta}^k c_{\mathbf{R}\alpha}^l \frac{e_0^2}{4\pi\epsilon_0\epsilon_r |\mathbf{R} - \mathbf{R}'|}. \quad (1)$$

The labels i, j, k, l refer either to electron or to hole states in case of the repulsive electron-electron and hole-hole interaction, or i, l label electron and j, k hole states for the attractive electron-hole interaction. The considerably smaller matrix elements of the electron-hole exchange interaction are neglected. The electronic charge and the vacuum dielectric constant are denoted by e_0 and ϵ_0 , respectively. We use the InN dielectric constant $\epsilon_r = 8.4$ according to Ref. 15 since the wave functions are almost completely confined inside the QD.

For the calculation of dipole matrix elements $\mathbf{d}_{ij}^{eh} = e_0 \langle \psi_i^e | \mathbf{r} | \psi_j^h \rangle$, the explicit structure of the localized orbitals is required as the dipole-operator has mainly local character. Standard Slater orbitals¹⁹ have been used in earlier calculations²⁰ within orthogonal TB models. While they include the correct symmetry properties, the missing orthogonality limits their applicability. To overcome this problem, we use numerically orthogonalized Slater orbitals. To properly treat the slight non-locality of the dipole operator²¹ and the anion-cation structure of the crystal, the matrix elements are calculated including up to second nearest neighbors. The only relevant dipole matrix elements are $\mathbf{e} \mathbf{d}_{sp_x}^{eh} = \mathbf{e} \mathbf{d}_{sp_y}^{eh}$ and $\mathbf{e} \mathbf{d}_{p_x s}^{eh} = \mathbf{e} \mathbf{d}_{p_y s}^{eh}$, where $\mathbf{e} = 1/\sqrt{2}(1, 1, 0)$ denotes the light polarization vector. All other matrix elements vanish due to the overall symmetry of the connected one-particle states^{22,23}. The resulting optical selection rules are in strong contrast to what is known from many other III-V and II-VI heterostructures and cannot be explained within an one-component effective-mass approach^{6,24}.

The single-particle states and Coulomb interaction matrix elements are used in the FCI calculations to determine the multi-exciton states. In a second step, Fermi's golden rule is evaluated for dipole transitions between these Coulomb-correlated states in order to obtain the multi-exciton emission spectra^{5,6}. The results for an initial filling of the dot with one up to six excitons are depicted in Fig. 2 with (solid line) and without (dotted line) the piezoelectric field. In the emission spectra two clusters of peaks are clearly visible, one on the high energy side, $\hbar\omega > 1.24\text{eV}$, and one on the low energy side, $\hbar\omega < 1.3\text{eV}$ (explicit numbers given in the text refer to the results including the piezoelectric field). As a characteristic feature, the high (low) energy transitions originate from a recombination process involving an electron (hole) in an excited state and a hole (electron) in the ground state. As the dipole matrix element d_{ss}^{eh} is negligible and the exciton and biexciton ground states are dominated by configurations where all the carriers are in the s-shell, the corresponding transitions $1X \rightarrow 0X$ and $2X \rightarrow 1X$ remain dark. The gap between the two sets of clusters is, to a first approximation, given by the difference in the involved one-particle energies, which is then renormalized by the Coulomb interaction. In a free particle picture each of the two clusters would collapse to one line. The splitting within the clusters can be attributed to transitions with different spin configurations of the final states. These configurations are energetically sepa-

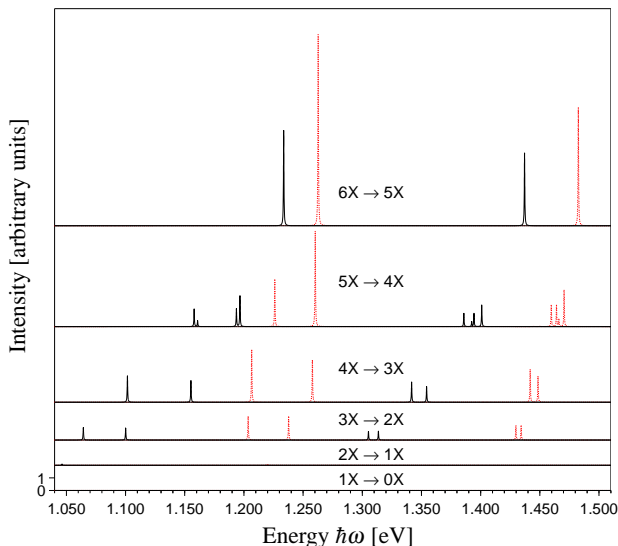


FIG. 2: (Color online). Emission spectra for a quantum dot with different number of excitons, with (solid line) and without (dotted line) piezoelectric field. Initial states are ground states with total spin z -component $S_z = 0$.

rated by approximate integer multiples of the Coulomb exchange integrals $V_{sp_x,y,sp_x,y}^{eeee} \approx 18$ meV for the low energy cluster, and $V_{sp_x,y,sp_x,y}^{hhhh} \approx 4$ meV for the high energy cluster. For clarification let us consider the $3X \rightarrow 2X$ transition. The $3X$ ground state is dominated by configurations with both electrons and holes having two carriers in the s - and one in the p -shell. Recombination of the p -electron (hole) with the s -hole (electron) leaves behind two electrons (holes) in the s -shell as well as one hole (electron) in the s -shell and one in the p -shell. The

latter can either form a singlet or a triplet state, which leads to a splitting of around 8 meV (36 meV), and is in accordance with the FCI-calculation. As the number of e - h -pairs is increased one observes an overall blue shift of the transitions. This shift is less pronounced without the piezoelectric field and can be explained in terms of the Hartree-Fock contributions to the interaction. The in general somewhat larger peak height of the low-energy transition is explained by the fact that the involved dipole matrix element $d_{sp_x,y}^{eh}$ is larger than $d_{p_x,y,s}^{eh}$, which enters the high energy transitions.

The inclusion of the piezoelectric field for the strained wurtzite crystal structure gives rise to a QCSE which creates a strong (about 220 meV) redshift of the one-particle gap energy. Additionally, the Coulomb matrix elements are strongly modified and the oscillator strengths are approximately halved due to the spatial separation of electron and hole wave functions.

In conclusion, we successfully combined two state-of-the-art approaches, the atomistic tight-binding model and full configuration-interaction calculations, to investigate the optical properties of the technologically very promising InN/GaN QD system. Multi-exciton emission spectra are calculated with microscopically determined input parameters, which reveal the strong influence of bandmixing effects on the optical transitions between the Coulomb correlated many-particle states. As an important consequence for future optoelectronic applications we predict vanishing exciton and biexciton ground state emission for small lens-shaped InN/GaN QDs.

We acknowledge financial support by the Deutsche Forschungsgemeinschaft and a grant for CPU time from the NIC at the Forschungszentrum Jülich.

- ¹ S. C. Jain, M. Willander, J. Narayan, and R. V. Overstraeten, *J. Appl. Phys.* **87**, 965 (2000).
- ² I. Vurgaftman and J. R. Meyer, *J. Appl. Phys.* **94**, 3675 (2003).
- ³ R. Santropete, B. Koiller, R. B. Capaz, P. Kratzer, Q. K. K. Liu, and M. Scheffler, *Phys. Rev. B* **68**, 235311 (2003).
- ⁴ S. Schulz and G. Czycholl, *Phys. Rev. B* **72**, in press (2005).
- ⁵ A. Barenco and M. A. Dupertuis, *Phys. Rev. B* **52**, 2766 (1995).
- ⁶ N. Baer, P. Gartner, and F. Jahnke, *Eur. Phys. J. B* **42**, 231 (2004).
- ⁷ S.-H. Wei and A. Zunger, *Appl. Phys. Lett.* **69**, 2719 (1996).
- ⁸ J. C. Slater and G. F. Koster, *Phys. Rev.* **94**, 1498 (1954).
- ⁹ D. Fritsch, H. Schmidt, and M. Grundmann, *Phys. Rev. B* **69**, 165204 (2004).
- ¹⁰ G. L. Zhao, D. Bagayoko, and T. D. Williams, *Phys. Rev. B* **60**, 1563 (1999).
- ¹¹ S. Sapra and D. D. Sarma, *Phys. Rev. B* **69**, 125304 (2004).
- ¹² S. De Rinaldis, I. D'Amico, and F. Rossi, *Appl. Phys. Lett.*

- 81**, 4236 (2002).
- ¹³ A. D. Andreev and E. P. O'Reilly, *Phys. Rev. B* **79**, 521 (2001).
- ¹⁴ T. Saito and Y. Arakawa, *Physica E* **15**, 169 (2002).
- ¹⁵ J.-J. Shi and Z.-Z. Gan, *J. Appl. Phys.* **94**, 407 (2003).
- ¹⁶ F. D. Sala, A. D. Carlo, P. Lugli, F. Bernardini, V. Fiorentini, R. Scholz, and J. M. Jancu, *Appl. Phys. Lett.* **74**, 2002 (1999).
- ¹⁷ V. A. Fonoberov and A. A. Balandin, *J. Appl. Phys.* **94**, 7178 (2003).
- ¹⁸ S. J. Sun and Y. C. Chang, *Phys. Rev. B* **62**, 13631 (2000).
- ¹⁹ J. C. Slater, *Phys. Rev.* **36**, 57 (1930).
- ²⁰ S. Lee, J. Kim, L. Jönsson, J. W. Wilkins, G. W. Bryant, and G. Klimeck, *Phys. Rev. B* **66**, 235307 (2002).
- ²¹ K. Leung, S. Pokrant, and K. B. Whaley, *Phys. Rev. B* **57**, 12291 (1998).
- ²² A. Bagga, P. K. Chattopadhyay, and S. Ghosh, *Phys. Rev. B* **71**, 115327 (2005).
- ²³ M. Nirmal, D. J. Norris, M. Kuno, M. G. Bawendi, A. L. Efros, and M. Rosen, *Phys. Rev. Lett.* **75**, 3728 (1995).
- ²⁴ J. Li and J.-B. Xia, *Phys. Rev. B* **61**, 15880 (2000).